Available online at www.sciencedirect.com
SCIENCE DIRECT®
Comput. Methods Appl. Mech. Engrg. 194 (2005) 1405–1426
Computer methods in applied mechanics and engineering
www.elsevier.com/locate/cma

The effect of material and thickness variability on the buckling load of shells with random initial imperfections

Vissarion Papadopoulos *, Manolis Papadrakakis

Institute of Structural Analysis and Seismic Research, National Technical University of Athens, 9 Iroon Polytechneiou, Zografou Campus, Athens 15780, Greece

Received 25 July 2003; received in revised form 19 December 2003; accepted 30 January 2004

Abstract

The effect of material and thickness imperfections on the buckling load of isotropic shells is investigated in this paper. For this purpose, the concept of an initial 'imperfect' structure is introduced involving not only geometric deviations of the shell structure from its perfect geometry but also a spatial variability of the modulus of elasticity as well as the thickness of the shell. The initial geometric imperfections are described as a two-dimensional uni-variate (2D-1V) stochastic field with statistical properties that are either based on an available data bank of measured initial imperfections or assumed, in cases where no experimental data is available. In order to describe the non-homogeneous characteristics of the initial imperfections, the spectral representation method is used in conjunction with an autoregressive moving average model with evolutionary power spectra based on a statistical analysis of the experimentally measured imperfections. In cases where no experimental results is available, the initial imperfections are assumed to be homogeneous and their impact on the buckling load is investigated on the basis of 'worst'-case scenarios with respect to the correlation length parameters of the stochastic fields. The elastic modulus and the shell thickness are described as 2D-1V non-correlated homogeneous stochastic fields, while the stochastic stiffness matrix of the shell elements is formulated using the local average method. The Monte Carlo Simulation method is used to calculate the variability of the buckling load, while for the determination of the limit load of the shell, a stochastic formulation of the elastoplastic and geometrically non-linear TRIC facet triangular shell element is implemented.

Keywords: Non-linear shell finite element; Random imperfections; Spectral representation; Autoregressive model; Evolutionary spectra

* Corresponding author.
E-mail addresses: vpapado@central.ntua.gr (V. Papadopoulos), mpapadra@central.ntua.gr (M. Papadrakakis).

0045-7825/$ - see front matter © 2004 Elsevier B.V. All rights reserved.
doi:10.1016/j.cma.2004.01.043

1. Introduction

The buckling behaviour of shell structures is generally influenced by their initial imperfections, which occur during the manufacturing and construction stages. Thus, the analysis of imperfection sensitive shells has attracted the attention of many researchers in the past. Although these research efforts resulted in achieving predictions close to the experimental results, it was soon realized that the wide scatter in measured buckling loads of shell structures could only be approximated through modeling taking into account the randomness of the imperfect geometries. This variability of initial imperfections together with their pronounced influence on the load carrying capacity of shells has been proved to be responsible for the large scatter observed in the experimental results [1–4]. In addition to initial geometric imperfections, other sources of imperfections such as the variability of thickness, material properties, boundary conditions and misalignment of loading are also responsible for the reduction as well as the scatter of the buckling load of shell structures [2,3,5]. In the majority of studies these influencing parameters have not been treated as stochastic variables in a rational manner. An accurate prediction of the buckling behaviour of shells would therefore require a realistic description of all uncertainties involved in conjunction with a robust finite element formulation that can efficiently and accurately handle the geometric as well as physical non-linearities of shell type structures [6].

In the present paper the effect of material and thickness imperfections on the buckling load of isotropic shells is investigated. For this purpose, the concept of an initial 'imperfect' structure is introduced involving not only geometric deviations of the shell structure from its perfect geometry but also a spatial variability of the modulus of elasticity as well as of the thickness of the shell. These combined 'imperfections' are incorporated in an efficient and cost effective non-linear stochastic finite element formulation of the TRIC shell element [8,9] using the local average method for the derivation of the stochastic stiffness matrix, while the variability of the limit loads is obtained by means of the Monte Carlo Simulation (MCS) procedure.

In order to investigate the influence of the material and thickness variability on the buckling load of shells with random geometric imperfections, two types of shell structures are selected with criterion their buckling behaviour up to the limit point. The first type is a shallow hinged isotropic cylindrical panel with a point load at the mid of its top surface. This shell exhibits a limit point buckling with large pre-buckling deformation response and considerable influence of the physical non-linearities on its buckling behaviour. The second type is a thin-walled isotropic axially compressed cylinder, which exhibits a bifurcation buckling that occurs while the structure remains elastic. Therefore, the second type is selected as an example of an imperfection-sensitive structure in the sense that small deviations from its perfect geometry may result in a dramatic reduction in its buckling strength [7], while the first type was selected in order to investigate the effect of material and thickness variability on the buckling behaviour of a less sensitive to initial imperfections type of shell.

The analysis of shell structures exhibiting physical and geometric non-linearities has received considerable attention over the past years and it has been shown the importance of both types of non-linearities on the carrying capacity of these structures. In this work a layered elastoplastic constitutive model based on the von Mises yield criterion, the associated flow rule and isotropic hardening is adopted in conjunction with the geometrically non-linear shell element TRIC [10]. The main advantage of this formulation is that the elastoplastic stiffness matrix is formed on the natural coordinate system and can be expressed analytically for each layer. Then, the total natural tangent stiffness matrix is computed by adding together the tangent stiffness matrix of each layer. This formulation inherits a number of advantages associated with the natural mode method. This elastic–plastic large displacement formulation is therefore considered a robust and cost-effective platform for the accurate prediction of the buckling and post buckling behaviour of imperfect shells.

The initial geometric imperfections are described as a two-dimensional uni-variate (2D-1V) stochastic field. In the case of the axially compressed cylinder, the statistical properties of the stochastic field are based

on an available data bank of measured initial imperfections [11]. The resulting stochastic field is clearly a non-homogeneous stochastic field with substantially varying first and second order properties. In the present study, the spectral representation method together with an autoregressive moving average model with evolutionary power spectra is used for the description of the non-homogeneous characteristics of the stochastic field [12–14]. This approach is adopted because it can be easily implemented as a straightforward extension of the well-established spectral representation method applied for the description of homogeneous fields. In the case of the hinged isotropic cylindrical panel, the initial imperfections are assumed to be homogeneous and their impact on the buckling load is investigated on the basis of 'worst'-case scenarios with respect to the correlation length parameters of the stochastic fields. In all cases, the elastic modulus and the shell thickness are described as two-dimensional uni-variate non-correlated homogeneous stochastic fields with assumed statistical properties.

In this work the efficiency of the proposed methodology is demonstrated in realistic problems, where the influence of the material and thickness variability on the buckling load of shells with random geometric imperfections is investigated in the presence of both geometric and physical non-linearities. The numerical tests performed demonstrate the decisive role that the material and thickness variability play in the buckling behaviour of both imperfection-sensitive and imperfection-insensitive shell structures. Furthermore, it is found that predictions of the scatter of the buckling load reasonably close to the experimental results can be obtained provided that the material and thickness imperfections are incorporated in a rational manner to the model of initial geometric imperfections.

2. Finite element formulation

The finite element simulation is performed with the triangular element TRIC, which is based on the natural mode method. The TRIC shear-deformable facet shell element is a reliable and cost-effective element suitable for linear and non-linear analysis of thin and moderately thick isotropic as well as composite plate and shell structures. For the sake of completeness a brief description of the TRIC shell element is given in this section. Extensive reports on the formulation of TRIC may be found in [8–10].

2.1. The TRIC shell element

The element has 18 degrees of freedom (6 per node) and hence 12 natural straining modes (Fig. 1). Three natural axial strains and natural transverse shear strains are measured parallel to the edges of the triangle. The stiffness is contributed by deformations only and not by the associated rigid body motions. The natural stiffness matrix can be produced from the statement of variation of the strain energy with respect to the natural coordinates.

The geometric stiffness is based on large deflections but small strains and consists of two parts: A simplified geometric stiffness matrix generated by the rigid-body movements of the element and the natural geometric stiffness matrix due to the coupling between the axial forces and the symmetric bending modes (stiffening or softening effect). To construct the geometric stiffness we consider small rigid-body rotational increments about the local Cartesian axes. These rigid-body rotational increments correspond to nodal Cartesian moments along the same axes. Using the fact that the resultants of all forces produced by rigid-body motion must vanish, we arrive at the expression for the local rigid-body rotational simplified geometric stiffness. The term simplified refers to the fact that only the middle plane axial natural forces are included in the stiffness matrix, which fully represent the pre-stress state within the material. Once the simplified geometric stiffness is formed it may transformed to the global coordinate system. In addition to the geometric stiffness corresponding to the rigid-body movements of the element, an approximate

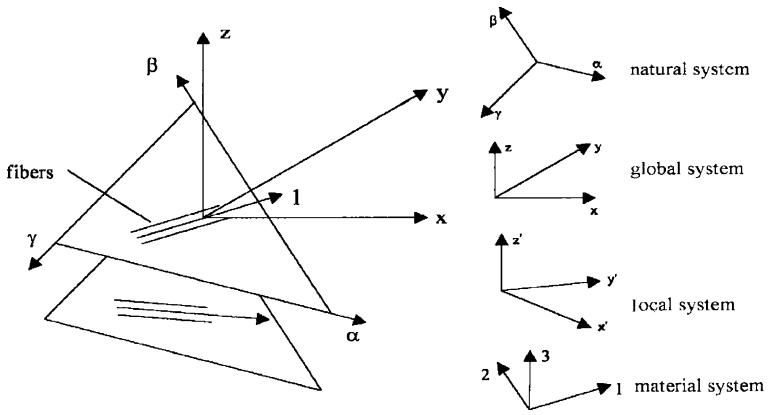

Fig. 1. The multilayer triangular TRIC element; coordinate systems.

natural geometric stiffness arising from the coupling between the axial forces and the symmetric bending mode (stiffening or softening effect) is also considered.

The elastoplastic constitutive matrix is established by obtaining the relation between the natural strain and stress increments for each layer r within a given load step:

$$\mathrm{d}\sigma_c^r = \left[\kappa_{ct}^{\mathrm{el}} - \frac{1}{H + s_{\mathrm{N}}^{\mathrm{t}}\kappa_{ct}^{\mathrm{el}}s_{\mathrm{N}}}(\kappa_{ct}^{\mathrm{el}}s_{\mathrm{N}})(\kappa_{ct}^{\mathrm{el}}s_{\mathrm{N}})^{\mathrm{t}}\right]^r \mathrm{d}\gamma_t^r, \tag{1}$$

where H is the hardening parameter and s_{N} is obtained by the normality flow rule as

$$s_{\mathrm{N}} = \frac{\partial F}{\partial \sigma_c} = \left[\frac{\partial F}{\partial \sigma_{c\alpha}} \quad \frac{\partial F}{\partial \sigma_{c\beta}} \quad \frac{\partial F}{\partial \sigma_{c\gamma}}\right]^{\mathrm{t}} \tag{2}$$

and the expression in brackets corresponds to the elastoplastic material stiffness matrix $\kappa_{ct}^{\mathrm{el-pl}}$ valid for every layer r:

$$[\kappa_{ct}^{\mathrm{el-pl}}]^r = \left[\kappa_{ct}^{\mathrm{el}} - \frac{1}{H + s_{\mathrm{N}}^{\mathrm{t}}\kappa_{ct}^{\mathrm{el}}s_{\mathrm{N}}}(\kappa_{ct}^{\mathrm{el}}s_{\mathrm{N}})(\kappa_{ct}^{\mathrm{el}}s_{\mathrm{N}})^{\mathrm{t}}\right]^r. \tag{3}$$

The natural elastoplastic stiffness of the element is obtained by summing up the natural elastoplastic layer stiffnesses of the element. A full description of the linear elastic, geometric and elastoplastic stiffness matrix of the TRIC shell element can be found in [8–10], respectively.

3. Description of initial imperfect geometry

The imperfect geometry of shell structures can in general be accurately represented as a 2D-1V stochastic field. In the case of the axially compressed cylinder, the statistical properties of the stochastic field are based on the data bank of measured initial imperfections by Arbocz and Abramovich [11]. The resulting stochastic field is clearly a non-homogeneous stochastic field with substantially varying first and second order properties.

Samples of the stochastic fields with statistical properties equivalent to the measured ones can generally be obtained by using the spectral representation method, the Karhunen–Loéve expansion or some other method. In the present study, the spectral representation method together with an autoregressive moving average model with evolutionary power spectra is used for the description of the non-homogeneous char-

acteristics of the stochastic field. The estimation of the evolutionary spectrum from the real data is accomplished using a standard moving window technique. The spectral representation with evolutionary power approach was selected because it can be easily implemented as a straightforward extension of the well-established spectral representation method used for modeling of homogeneous fields. The use of this approach to model and simulate non-stationary processes and non-homogeneous fields dates back to the 1970s and is very well established [12–14]. Using this approach, the decomposition of the covariance matrix required by the Karhunen–Loéve decomposition is avoided, which is most beneficial in cases where a large number of terms is required in the Karhunen–Loéve expansion for the accurate representation of the stochastic field.

From the statistical analysis of the measured imperfections it occurs that the assumption of normality is in accordance with the experimental data. Therefore, the imperfect geometry represented by the variation of the radius of the structure can be represented as a 2D-1V non-homogeneous Gaussian stochastic field:

$$r(x,y) = R + a_0(x,y) + f_1(x,y), \tag{4}$$

where $r(x,y)$ is the varying initial radius at each point of the structure, R is the radius of the perfect cylinder, $a_0(x,y)$ is the mean function of the imperfections with respect to the perfect geometry of the shell and $f_1(x,y)$ is a zero mean non-homogeneous Gaussian stochastic field.

In the case of the hinged isotropic cylindrical panel considered in this study, the initial imperfections are assumed to be zero-mean and homogeneous and their impact on the buckling load was investigated in the basis of 'worst'-case scenarios with respect to the correlation length parameters of the stochastic fields, which control the shape of the imperfections.

4. Stochastic stiffness matrix

The modulus of elasticity as well as the thickness of the structure are also considered in the present study as 'imperfections', due to their spatial variability. Therefore, these parameters are also described by two independent 2D-1V homogeneous stochastic fields:

$$E(x,y) = E_0[1 + f_2(x,y)], \tag{5}$$

$$t(x,y) = t_0[1 + f_3(x,y)], \tag{6}$$

where E_0 is the mean value of the elastic modulus, t_0 is the mean thickness of the structure and $f_2(x,y)$, $f_3(x,y)$ are two zero mean Gaussian homogeneous stochastic fields corresponding to the variability of the modulus of elasticity and the thickness of the shell, respectively.

The stochastic stiffness matrix of the shell element is derived using the local average method. In a recent study by Argyris et al. [15] it was shown that for the shell type structures examined in this work, the local average method is not only superior to the weighted integral method in terms of simplicity and computational efficiency, but it was found to be equally effective in terms of accuracy of the computed results.

5. Spectral representation

In the present paper the generation of sample functions is performed using the spectral representation method [16]. The simulation points of the stochastic fields are located at the center of gravity of the TRIC shell elements. Therefore, the stochastic fields are simulated in non-uniformly spaced points of the structure. For this reason, the series of cosines formula is chosen for the simulation of the stochastic fields instead of the Fast Fourier Transform (FFT) which requires that the stochastic field is simulated at uniformly

spaced points. In addition, the FFT is not applicable in case that autoregressive models with evolutionary power spectra are incorporated into the simulation algorithm of the spectral representation method.

5.1. 2D-1V homogeneous stochastic fields

The series of cosines formula for the simulation of a 2D-1V homogeneous stochastic field is as follows:

$$f^{(i)}(x_1,x_2)=\sqrt{2}\sum_{n_1=0}^{N_1-1}\sum_{n_2=0}^{N_2-1}[A^{(1)}_{n_1n_2}\cos(\kappa_{1n_1}x_1+\kappa_{2n_2}x_2+\phi^{(1)(i)}_{n_1n_2})+A^{(2)}_{n_1n_2}\cos(\kappa_{1n_1}x_1-\kappa_{2n_2}x_2+\phi^{(2)(i)}_{n_1n_2})], \tag{7}$$

where $\phi^{(j)(i)}_{n_1n_2}$, $j=1,2$ represent the realization for the (i) simulation of the independent random phase angles uniformly distributed in the range $[0,2\pi]$. $A^{(1)}_{n_1n_2}$, $A^{(2)}_{n_1n_2}$ are defined as

$$A^{(1)}_{n_1n_2}=\sqrt{2S_{f_0f_0}(\kappa_{1n_1},\kappa_{2n_2})\Delta\kappa_1\Delta\kappa_2}, \tag{8a}$$

$$A^{(2)}_{n_1n_2}=\sqrt{2S_{f_0f_0}(\kappa_{1n_1},-\kappa_{2n_2})\Delta\kappa_1\Delta\kappa_2}, \tag{8b}$$

where

$$\kappa_{1n_1}=n_1\Delta\kappa_1,\quad \kappa_{2n_2}=n_2\Delta\kappa_2, \tag{9}$$

$$\Delta\kappa_1=\frac{\kappa_{1u}}{N_1},\quad \Delta\kappa_2=\frac{\kappa_{2u}}{N_2}, \tag{10}$$

$$n_1=0,1,\ldots,N_1-1,\quad n_2=0,1,\ldots,N_2-1, \tag{11}$$

N_j, $j=1,2$, are the numbers of intervals in the discretization of the spectrum and κ_{ju}, $j=1,2$, are the upper cut-off wave numbers which define the active region of the power spectrum $S_{f_0f_0}$ of the stochastic field. The last implies that the power spectral density function $S_{f_0f_0}(\kappa_1,\kappa_2)$, for either mathematical or physical reasons, is assumed to be zero outside the region defined by

$$-\kappa_{1u}\leqslant\kappa_1\leqslant\kappa_{1u}\ \text{ and }\ -\kappa_{2u}\leqslant\kappa_2\leqslant\kappa_{2u}. \tag{12}$$

The two-sided power spectral density function $S_{f_0f_0}$ is assumed to correspond to an autocorrelation function of exponential type and is given by

$$S_{f_0f_0}(\kappa_1,\kappa_2)=\frac{\sigma_f^2}{4\pi}b_1b_2\exp\left[-\frac{1}{4}(b_1^2\kappa_1^2+b_2^2\kappa_2^2)\right], \tag{13}$$

where σ_f denotes the standard deviation of the stochastic field and b_1, b_2 denote the parameters that influence the shape of the spectrum which are proportional to the correlation distances of the stochastic field along the x_1, x_2 axes, respectively.

Using Eq. (7), a large number N_{samp} of sample functions are produced, leading to the generation of a set of stochastic stiffness matrices. The associated structural problem is solved N_{samp} times, while the response variability can finally be calculated by taking the response statistics of the N_{samp} simulations.

5.2. 2D-1V non-homogeneous stochastic fields

For the simulation of a 2D-1V non-homogeneous stochastic field, the series of cosines formula given in Eq. (7) becomes as follows:

$$f^{(i)}(x_1,x_2)=\sqrt{2}\sum_{n_1=0}^{N_1-1}\sum_{n_2=0}^{N_2-1}[A^{(1)}_{n_1n_2}\cos(\kappa_{1n_1}x_1+\kappa_{2n_2}x_2+\phi^{(1)(i)}_{n_1n_2})+A^{(2)}_{n_1n_2}\cos(\kappa_{1n_1}x_1-\kappa_{2n_2}x_2+\phi^{(2)(i)}_{n_1n_2})], \quad (14)$$

where, $A^{(1)}_{n_1n_2}$, $A^{(2)}_{n_1n_2}$ are now functions of not only the wave numbers but also of the positions x_1, x_2:

$$A^{(1)}_{n_1n_2}=\sqrt{2S^E(\kappa_{1n_1},\kappa_{2n_2},x_1,x_2)\Delta\kappa_1\Delta\kappa_2}, \quad (15a)$$

$$A^{(2)}_{n_1n_2}=\sqrt{2S^E(\kappa_{1n_1},-\kappa_{2n_2},x_1,x_2)\Delta\kappa_1\Delta\kappa_2}, \quad (15b)$$

where $S^E(\kappa_{1n_1}, \kappa_{2n_2}, x_1, x_2)$ is the auto evolutionary power spectrum given by

$$S^E(\kappa_1,\kappa_2,x_1,x_2)=\frac{\int_{x_2-b}^{x_2+b}\int_{x_1-a}^{x_1+a}f(x_1,x_2)\exp[-2\pi i(\kappa_1x_1+\kappa_2x_2)]\,dx_1\,dx_2}{8\pi ab}. \quad (16)$$

The intervals $2a$ and $2b$ define the dimensions of the moving window of the sample from which the evolutionary spectrum is estimated at each point of the discretized structure.

6. Numerical examples

Two test examples are presented to demonstrate the efficiency as well as the applicability of the proposed methodology. The first example is the shallow hinged isotropic cylindrical panel shown in Fig. 2. This example is chosen because it exhibits a highly non-linear behaviour with considerable influence of the physical non-linearities on the overall structural response. In a previous work by Papadopoulos and Papadrakakis [17] the same example was investigated considering only geometric non-linearities. In the present study this investigation is extended to incorporate the elastoplastic behaviour of this structure where the dominant role of the elastoplastic behaviour in the buckling analysis of the imperfect cylindrical panel is demonstrated.

The second example is the axially compressed cylinder of Fig. 13. For this example, an extensive investigation was performed by Schenk and Schueller [3], which was also based on the data bank of Arbocz and Abramovich [11]. An extension to this investigation that includes, not only the initial imperfect geometry

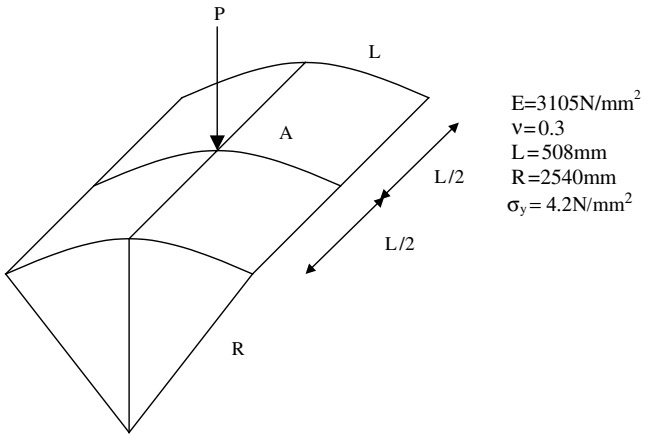

Fig. 2. Geometry, and material data of the cylindrical panel.

but also the variability of the modulus of elasticity as well as the thickness of the cylinder, is presented in this paper. The important role that these additional imperfection parameters play in the buckling behaviour of the cylinder is demonstrated.

6.1. The hinged isotropic cylindrical panel

The loading as well as the geometric and material properties of the perfect shell is also shown in Fig. 2. The curve edge nodes of the panel are assumed to be free in all directions while the nodes along the sides are hinged (fixed against translation). The material is considered to be elastic-perfectly plastic. The geometrically non-linear elastic as well as elastoplastic response of point A of the perfect cylinder with respect to the applied vertical load P, is shown in Fig. 3, where the cylindrical panel is discretized with a 21×21 mesh of 400 TRIC shell elements. A mesh convergence study for this particular example is presented in a previous investigation [9] where the computational efficiency of the TRIC element in non-linear shell analysis was demonstrated. For the discretization of the stochastic fields, the same mesh used for the finite element analysis is implemented since it is a fraction of the correlation length parameters adopted in this example. Thus, it is considered dense enough for the accurate representation of the fluctuations of the stochastic fields [18]. The ultimate load of the perfect configuration is found to be $P_u = 2205\,\text{N}$ for the elastic shell and $P_u = 1.240\,\text{N}$ for the elastoplastic.

6.1.1. Initial geometric imperfections

Both 1D and 2D stochastic imperfections are introduced to the model in order to investigate their effect on the buckling load of the panel. The thickness of the shell is considered to be equal to the height h at the apex, i.e. $t = 12.7\,\text{mm}$. For all cases, the standard deviation σ_f of the stochastic field of the imperfections is assumed to be $\sigma_f = 0.02h$, where h is the height at the apex of the cylindrical panel. Since no experimental data of initial imperfections is available for this specific type of structure, a parametric study was performed in a previous investigation by Papadopoulos and Papadrakakis [17], with respect to the correlation lengths of the stochastic fields in both x, y directions. The outcome of the parametric study was the evaluation of the 'worst' imperfection mode of the shell, which led to the estimation of the lower bound of the buckling load of the shell. This information is most valuable for the safe design of shells against buckling.

The 1D stochastic imperfections are introduced in the free edge direction. The 'worst' imperfection mode for this case corresponds to a correlation length parameter $b_1 = 50\,\text{mm}$ [17]. For this correlation length parameter, a Monte Carlo Simulation procedure is performed to obtain the variability of the critical load factor of the panel. The Monte Carlo Simulation is performed using a sample size $N_{\text{samp}} = 100$, which is considered sufficient for an accurate estimation of the mean value and the standard deviation of the buck-

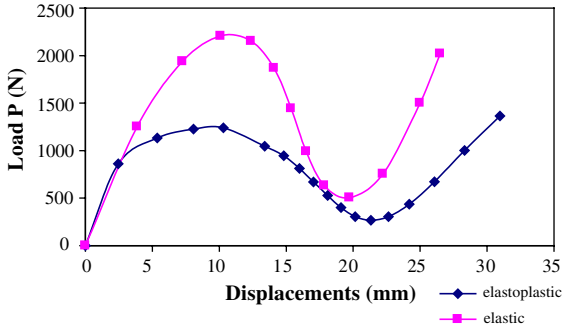

Fig. 3. Central load–displacement curve of the perfect cylindrical panel for $t = 12.7\,\text{mm}$.

ling loads. In Fig. 4 one sample function generated for this correlation parameter b_1 is presented, while Fig. 5 presents the histograms of the buckling loads for the same value of the parameter b_1, with and without physical non-linearities. In the case where both geometric and physical non-linearities are included, the mean value of the buckling load is found to be 1206 N, while the coefficient of variation (Cov) is found to be 12%. The lowest buckling load for this case is estimated at 930 N. In the case in which only geometric non-linearities are included, the mean value of the buckling load was found in [17] to be 2050 N and Cov 24%. In this case the lowest buckling load was estimated at 1060 N.

The same steps are followed for the case of the 2D stochastic imperfections. It is assumed that the correlation lengths in both x and y directions are equal, $b_1 = b_2$, since there are no specific manufacturing procedures or boundary conditions that would indicate a different assumption. The 'worst' imperfection mode for this case corresponds to a correlation length parameter $b_1 = b_2 = 250$ mm [17]. In Fig. 6 one sample function generated for this correlation parameter is presented, while Fig. 7 presents the histograms of

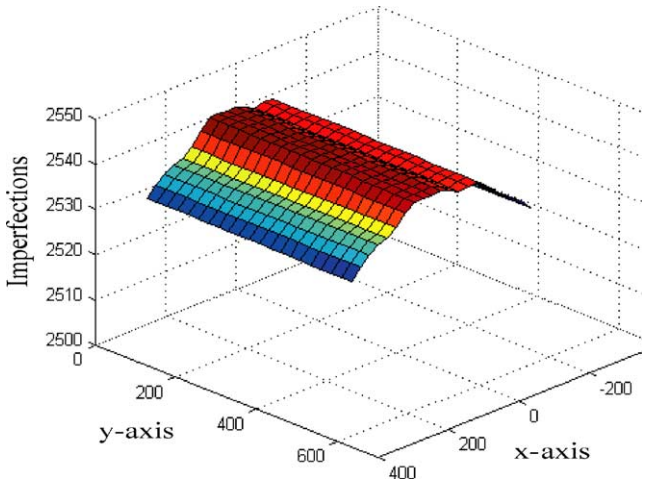

Fig. 4. One sample function of 1D initial imperfection shapes of the cylindrical panel for $\sigma_f = 0.10$ and $b_1 = 50$ mm.

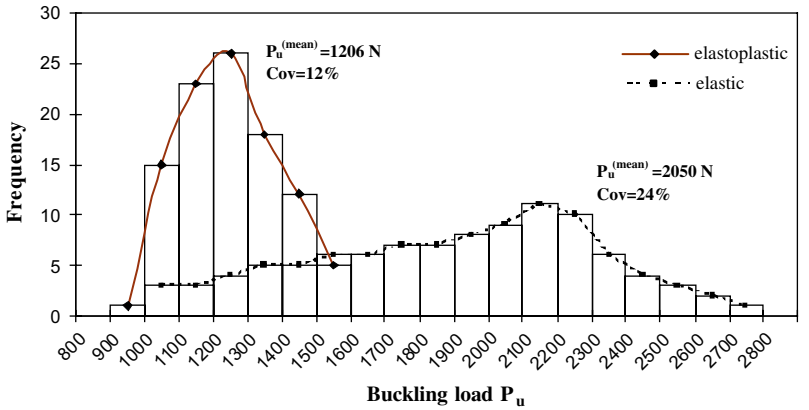

Fig. 5. Histograms of the critical load factor P_u for 1D stochastic imperfections ($\sigma_f = 20\%$ and $b_1 = 50$ mm).

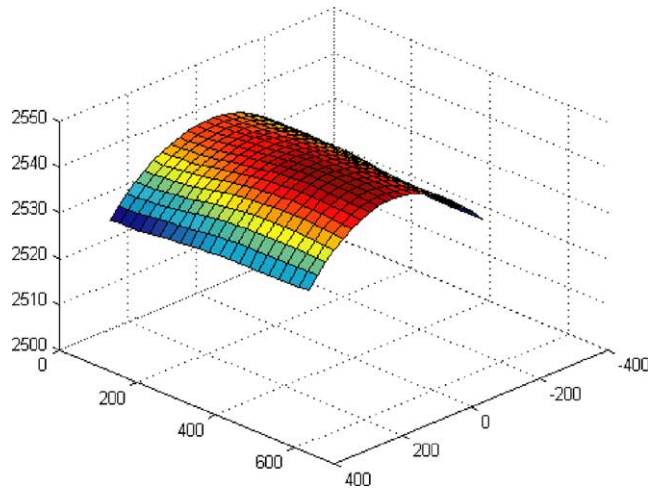

Fig. 6. 2D initial imperfection shape for $\sigma_f = 0.20$ and correlation length $b_2 = 250$ mm.

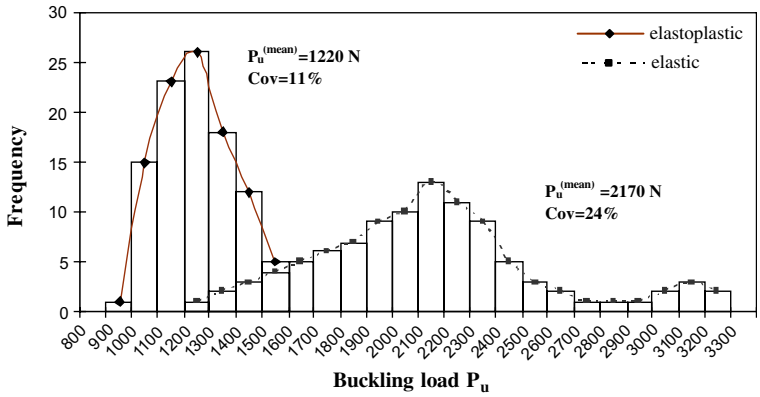

Fig. 7. Histograms of the critical load factor P_u for 2D stochastic imperfections ($\sigma_f = 20\%$ and $b_1 = b_2 = 250$ mm).

the buckling loads for the 'worst' value of the correlation length parameter, with and without physical non-linearities. In the case where both geometric and physical non-linearities are included, the mean value of the buckling load is found to be 1.220 N with a Cov 11%. The lowest buckling load is estimated at 900 N for this case. In the case in which only geometric non-linearities are included, the mean value of the buckling load was found to be 2170 N and the Cov 24% [17]. In this case the lowest buckling load was estimated at 1200 N.

From the comparison of Figs. 5 and 7 it can be seen that the behaviour of the panel for 1D and 2D stochastic geometric imperfections is very similar. For both cases, a reduction of about 45% of the mean value of the buckling loads can be observed in the elastoplastic model with respect to the elastic one. This reduction of the buckling loads is of the same magnitude with the reduction observed in Fig. 3 for the perfect configuration. It can also be observed that the scatter of the buckling loads for the elastoplastic model is smaller than the scatter observed for the elastic one. The coefficient of variation is found to be 12% for the elastoplastic model, which amounts only 50% of the coefficient of variation of the elastic model. Conse-

quently, the lowest buckling load of the elastoplastic model is only 10% lower compared to the lowest buckling load of the corresponding elastic model. This reduction of the variability of the buckling loads for the elastoplastic model with respect to the elastic one can be explained by the fact that the elastoplastic non-linear behaviour of the panel is smoother compared to the elastic one, as can be seen in Fig. 3, due to the progressive spread of plasticity throughout the volume of the panel which makes the panel less sensitive to initial perturbations.

6.1.2. Combined geometric, material and thickness imperfections

The initial geometric imperfections are now introduced simultaneously to the model with material and thickness imperfections. For this purpose, the 'worst' imperfection modes and the corresponding correlation length parameters are depicted from [17]. For the combined imperfections all Monte Carlo simulations are performed using a sample size $N_{\text{samp}} = 1000$, as opposed to $N_{\text{samp}} = 100$ used in the previous cases, since a larger sample size is required for the accurate prediction of the 'exact' lowest buckling load of the panel. For the combined 1D variation of stochastic imperfections the value of $b_1 = 50$ mm is introduced for all imperfection parameters. Fig. 8 presents the histograms of the buckling loads with and without physical non-linearities, for this value of the parameter b_1. In the case where both geometric and physical non-linearities are included, the mean value of the buckling load and the coefficient of variation are found to be 1168 N and 16%, respectively, while the lowest buckling load is computed at 700 N. In the case in which only geometric non-linearities are included, the mean value of the buckling load and the coefficient of variation were found to be 1.230 N and 45%, respectively [17]. The lowest buckling load for this case was computed at 500 N.

From the comparison of Figs. 5 and 8, it can be observed that the buckling behaviour of the elastoplastic shell for the 1D combined imperfections remains more or less the same with respect to the stand-alone case (initial geometric imperfections only). From Fig. 8, it can be seen that a reduction of less than half of the coefficient of variation is computed in the elastoplastic model compared to the elastic one for the combined imperfections case, while the mean value of the buckling loads remains almost the same. In the stand-alone case (initial geometric imperfections only), as shown in Fig. 5, the elastoplastic behaviour resulted in a simultaneous reduction of both the coefficient of variation and the mean value of the predicted buckling loads by about 50%, compared to the elastic behaviour of the panel.

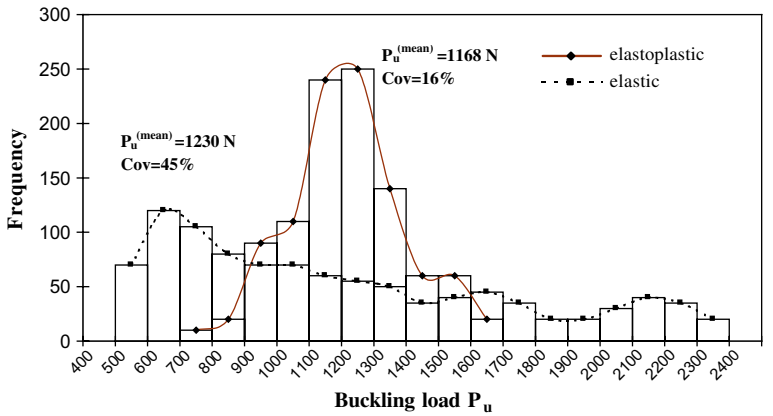

Fig. 8. Histograms of the critical load factor P_u for 1D variation of combined geometric, material and thickness imperfections ($\sigma_f = 20\%$).

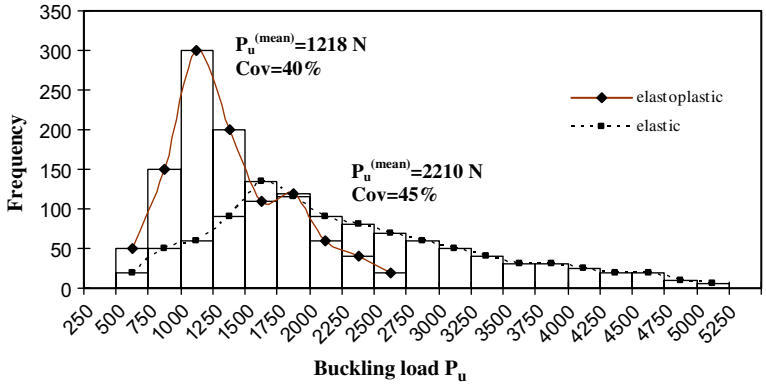

Fig. 9. Histograms of the critical load factor P_u for 2D variation of combined geometric, material and thickness imperfections ($\sigma_f = 20\%$).

For the 2D combined variation of stochastic imperfections the value of $b_1 = b_2 = 250$ mm is introduced to the initial geometric imperfections, while the value of $b_1 = b_2 = 2000$ mm is introduced to the variation of the modulus of elasticity and the thickness of the shell. Fig. 9 presents the histograms of the buckling loads for these values of the correlation length parameters, with and without physical non-linearities. In the case where both geometric and physical non-linearities are included, the mean value of the buckling load and the coefficient of variation are found to be 1218 N and 40%, respectively, while the lowest buckling load is computed at 500 N. In the case in which only geometric non-linearities are included, the mean value of the buckling load and the coefficient of variation were found to be 2210 N and 45%, respectively. In this case the lowest buckling load was computed at 500 N.

From Fig. 9 it can be observed that a reduction of about 50% of the mean value of the buckling loads is computed in the elastoplastic panel with respect to the elastic one for the combined imperfections case, while the coefficient of variation remains the almost the same (45%). From the comparison of Figs. 7 and 9 it can be seen that the introduction of 2D combined imperfections to the elastoplastic model increases four times the coefficient of variation of the buckling loads with respect to the stand-alone case. Therefore, the decrease of the variability of the buckling load of the elastoplastic panel with respect to the elastic one, which was exhibited in all 1D initial imperfection cases, is no longer observed in the case of the most realistic 2D combined stochastic initial imperfections.

6.1.3. Thin cylindrical panel

The previous investigations for the combined imperfections are repeated for the same cylindrical panel of Fig. 4 but with half its thickness ($t = 6.35$ mm). The non-linear response of point A of the perfect panel with respect to the applied vertical load P, is shown in Fig. 10. The ultimate loads of the perfect configuration with and without physical non-linearities are found to be $P_u = 390$ and 580 N, respectively. From this figure it can be observed that the elastoplastic behaviour of the thinner panel is smoother compared to the corresponding behaviour of the thick panel. For the 1D combined variation of stochastic imperfections the value of $b_1 = 50$ mm is introduced for all imperfection parameters. Fig. 11 presents the histograms of the buckling loads for this value of the parameter b_1 with and without physical non-linearities. In the case where both geometric and physical non-linearities are included the mean value of the buckling loads was computed at 330 N with Cov = 20%. The lowest buckling load for this case is computed at 210 N. In the case in which only geometric non-linearities are included, $P_u = 365$ N and Cov = 45%, while the lowest buckling load was computed at 120 N [15].

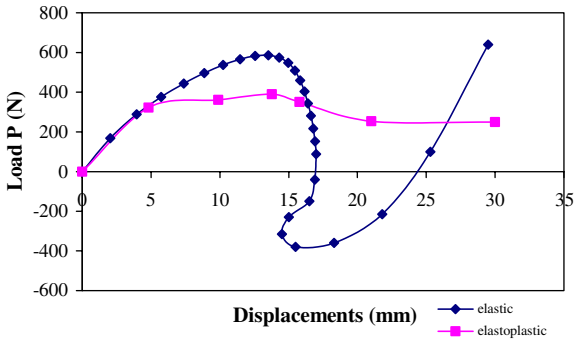

Fig. 10. Central load–displacement curve of the perfect cylindrical panel for $t = 6.35$ mm.

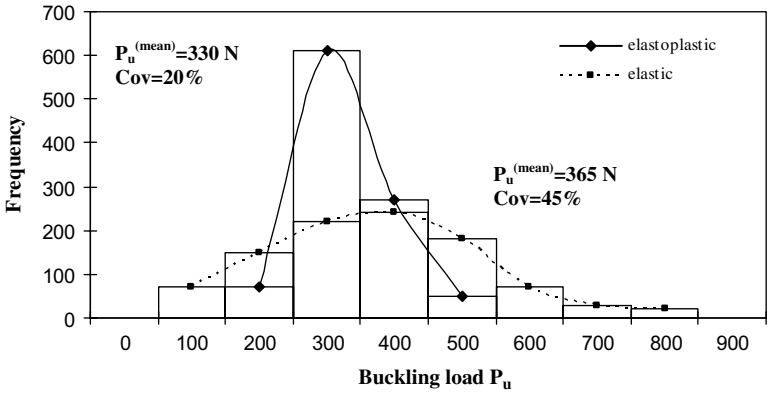

Fig. 11. Histograms of the critical load factor P_u for 1D variation of combined geometric, material and thickness imperfections ($\sigma_f = 20\%$ and $t = 6.35$ mm).

For the 2D combined variation of stochastic imperfections the values of $b_1 = b_2 = 250$ mm are introduced to the initial geometric imperfections, while the values of $b_1 = b_2 = 2000$ mm are introduced to the modulus of elasticity and the thickness of the shell. Fig. 12 presents the histograms of the buckling loads for these values of the correlation length parameters, with and without physical non-linearities. In the case where both geometric and physical non-linearities are included the mean value of the buckling loads was computed at 375 N with Cov = 45%. The lowest buckling load for this case is computed at 120 N. In the case in which only geometric non-linearities are included, $P_u = 480$ N and Cov = 50%, while the lowest buckling load was computed at 120 N.

From Fig. 11, it can be observed that a reduction of more than 50% in the coefficient of variation of the buckling loads is computed in the elastoplastic panel with 1D combined imperfections with respect to the elastic one, while the mean value of the buckling loads remains almost the same. From of Fig. 12, a reduction of about 20% in the mean value of the buckling loads of the elastoplastic panel with 2D combined imperfections can be observed, with respect to the elastic one, while the coefficient of variation remains almost the same (45%). In general, it can be deduced that the buckling behaviour of the thin cylindrical panel is qualitatively more or less the same to that of the behaviour of the thicker panel.

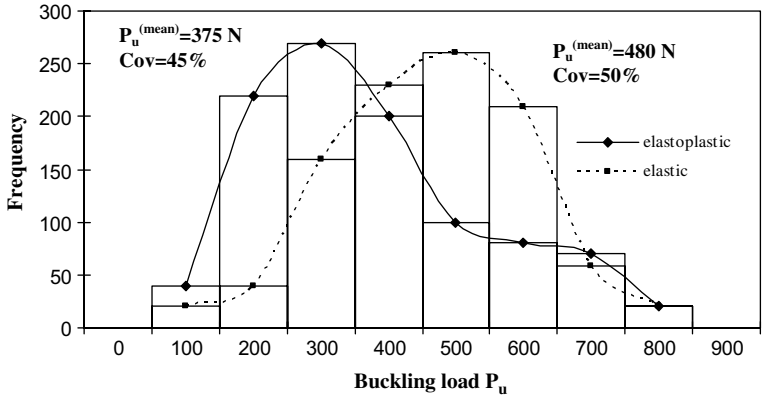

Fig. 12. Histogram of the critical load factor P_u for 2D variation of combined geometric, material and thickness imperfections ($\sigma_f = 20\%$ and $t = 6.35$ mm).

6.2. The axially compressed cylinder

The second selected example is the axially compressed cylinder of Fig. 13. The boundary conditions of the cylinder are specified according to [3]. The base edge nodes of the cylinder are fixed against all translations, fixed against rotations around the Y axis and free against rotations around the X and Z axis. The top edge nodes of the cylinder are fixed against X and Z translations, fixed against rotations around the Y axis, free against translations in the Y axis and free against rotations around axis X and Z.

For the simulation of the stochastic field that describes the geometric imperfections, first and second order statistical information is required. This information is obtained from statistical analysis of experimentally measured imperfections on seven copper electroplated cylindrical shells depicted from the data bank on initial imperfections of Arbocz and Abramovich [11]. The geometric and material properties of the cor-

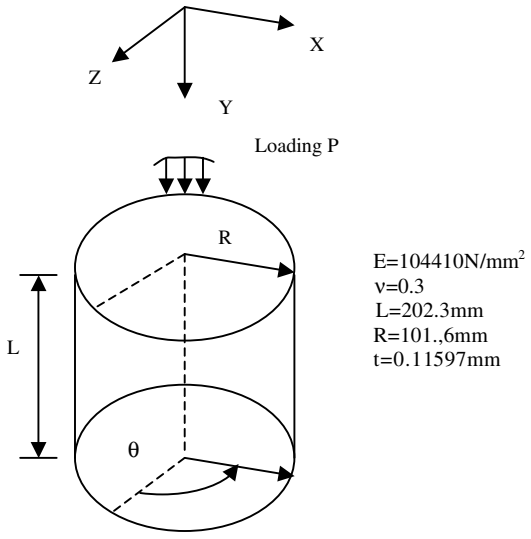

Fig. 13. Geometry and material data of the axially compressed cylinder.

responding perfect configurations of the shells as well as the experimental buckling loads are presented in Table 1. The average material and geometric properties used for the finite element model of the perfect cylinder are also shown in Fig. 13. A typical pattern of measured imperfections for shell A-7 is plotted in Fig. 14. From this figure it can be observed that the imperfections appear to be completely separate in the axial and the circumferential directions while the imperfections in the circumferential direction are one order of magnitude larger than those of the axial direction.

In order to obtain the first and second order properties of the imperfections, an origin for the coordinate system has to be defined. The value of the absolute maximum imperfection is selected as origin in both the axial and the circumferential direction, since in all specimens the absolutely maximum imperfection is located at one of the cylinder edges. Due to the assumed symmetry of the boundary conditions as well as of the loading, this origin is kept constant for all Monte Carlo simulations. The mean function $a_0(x, y)$ of the imperfections was calculated over the ensemble and plotted in Fig. 15. From this figure it can be observed that the mean value varies substantially along the two directions of the cylinder while, from the comparison of this figure with Fig. 14, it can be observed that first order properties of the imperfections are mainly responsible for the amplitudes as well as for the basic pattern of the imperfections.

As mentioned above, the patterns of the measured imperfections imply that a completely separate correlation structure exists in the axial and circumferential direction. This was also observed in [3] where a completely independent correlation structure was implemented. The evolutionary power spectrum adopted in the present study is also separate with respect to the two directions of the cylinder

$$S^E(\kappa_1, \kappa_2, x_1, x_2) = S_1^E(\kappa_1, x_1) S_2^E(\kappa_2, x_2), \tag{17}$$

Table 1
Geometry, material properties and experimental buckling loads of A-shells

Shell	R (mm)	t (mm)	L (mm)	E (N/mm^2)	$P(N)$
A-7	101.6	0.1140	203.20	10,4110	3036.4
A-8	101.6	0.1179	203.20	10,4800	3673.8
A-9	101.6	0.1153	203.20	10,1350	3724.8
A-10	101.6	0.1204	203.20	10,2730	3196.9
A-12	101.6	0.1204	209.55	10,4800	3853.0
A-13	101.6	0.1128	196.85	10,4110	3108.8
A-14	101.6	0.1110	196.85	10,8940	3442.9

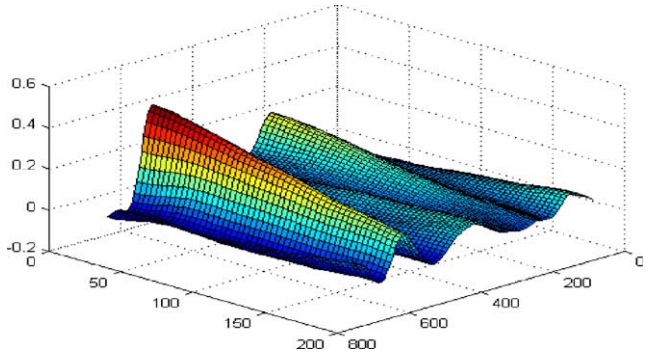

Fig. 14. Measured initial unfolded shape of shell A-7.

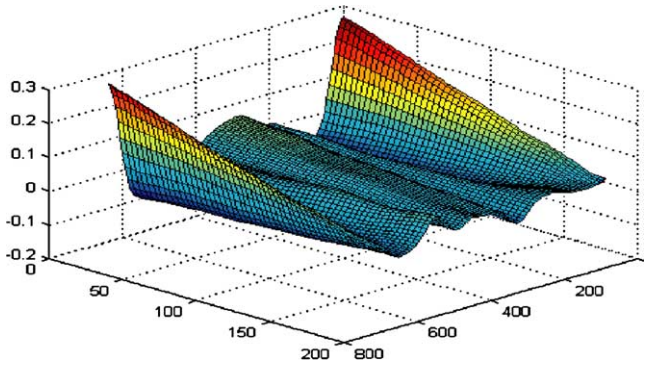

Fig. 15. Ensemble average of initial imperfections.

where $S_1^E(\kappa_1, x_1)$ and $S_2^E(\kappa_2, x_2)$ are two independent 1D spectra for the axial and circumferential direction, respectively.

Using Eq. (16), the separate evolutionary 1D spectra are evaluated over the sample and averaged over the ensemble. The length of the sample used for the calculation of the spectrum at each grid point of the structure is selected to be $a = 0.01L$ and $b = 0.01\pi R$ for the axial and the circumferential direction, respectively. The evolutionary power spectra along the directions of the cylinder are plotted in Fig. 16. From this figure it can be observed that the standard deviation varies substantially along the two directions of the cylinder, while the correlation length remains almost constant and equal to $b_1 \approx 0.6L$ for the axial and $b_2 \approx 0.06(2\pi R)$ for the circumferential direction. The same values for the correlation lengths were computed in [3] where homogeneity was temporarily assumed for this calculation.

In order to carry out accurately and efficiently the non-linear analyses of the imperfect cylinder required for the Monte Carlo simulation procedure, an optimum FE mesh size must be found that satisfies the following requirements: (i) accurate prediction of the buckling load(s) of the cylinder and (ii) accurate representation of the gradients of the stochastic initial imperfection field. For this purpose, a mesh convergence study of a quarter of the perfect cylinder is performed. Fig. 17 presents the predicted buckling loads for various mesh sizes. The predicted buckling load levels are normalized by the theoretical buckling load of the perfect cylinder

$$P_{\mathrm{u}}^{(\mathrm{perfect})} = \frac{Et^2}{R\sqrt{3(1-v^2)}}, \tag{18}$$

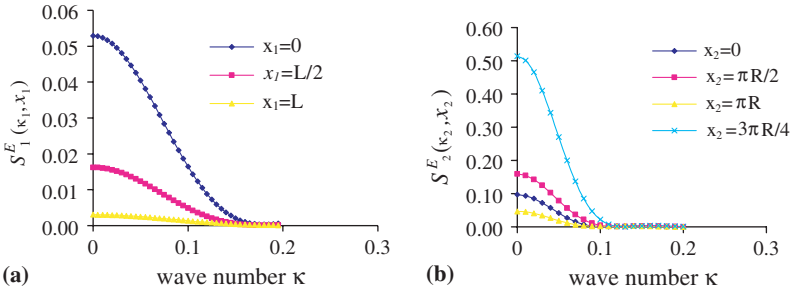

Fig. 16. Evolutionary power spectra of (a) axial direction and (b) circumferential direction of the cylinder.

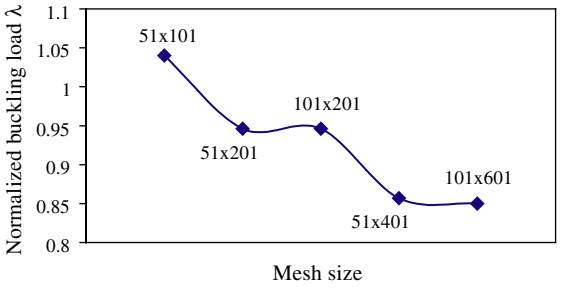

Fig. 17. Convergence behaviour of a quarter of the perfect cylinder.

which is found to be $P_u^{(perfect)} = 5350\,N$. The predicted critical buckling load is assumed to correspond to the load level at which the first negative eigenvalue of the tangent stiffness matrix of the structure appears.

From Fig. 17, it can be observed that 51 grid points are sufficient for the discretization of the axial direction, while 401 points are required in the circumferential direction for the accurate representation of the pre-buckling state of deformation, caused by the end boundary conditions of the cylinder as well as of the lowest buckling mode. The accurate representation of the pre-buckling state of deformation is of major importance, since it strongly affects the shapes of the buckling modes of the structure and hence, the level of the critical buckling load [3,19]. For this mesh size (51×401), the resulting finite element model has 120.000 degrees of freedom. It is obvious that the use of such a model in the context of a non-linear MCS procedure is an extremely computationally intensive task for the scope of the present paper. This is because the effect of material and thickness variability on the buckling load of the imperfect cylinder is investigated on the basis of a parametric study in which a number of Monte Carlo simulations has to be performed. Figs. 18 and 19 present the traces of the pre-buckling deformation predicted by the mesh of 51×101 and the mesh of 51×401 for the axial and circumferential direction, respectively. From these figures it can be seen that the deformed shapes predicted by the coarser mesh of the 51×101 nodal points are sufficiently close to the shapes predicted by the refined mesh of 51×401. For this reason, it is believed that the error in the prediction of the buckling load level ($\sim$15%) using the coarser mesh is a systematic discretization error, which will not affect the reliability of comparative studies for the buckling behaviour of the imperfect cylinder.

Fig. 20 shows a sample realization of the initial geometric imperfections generated by Eq. (14) for the FE mesh of 51×101. From this figure it can be seen that this FE mesh can sufficiently represent the gradients of the imperfect shape of the cylinder, since the mesh size used is a fraction of the correlation length of the

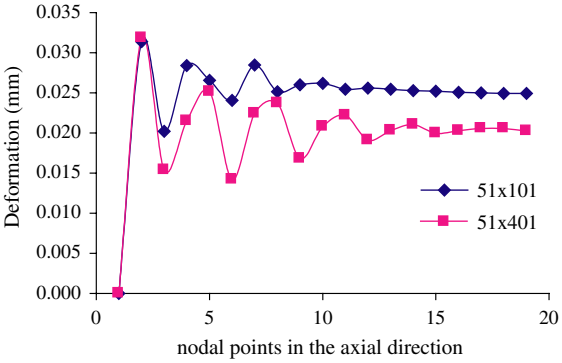

Fig. 18. Half axial trace of pre-buckling deformation of the perfect cylinder.

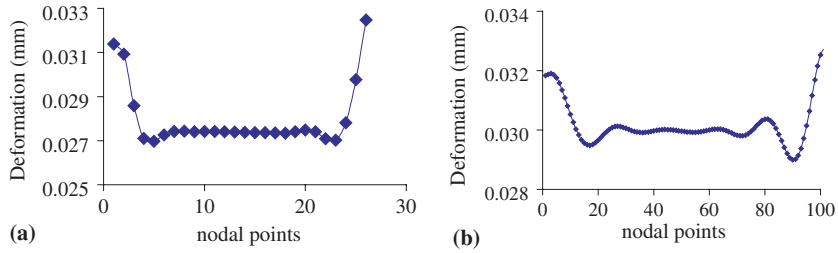

Fig. 19. Circumferential trace of pre-buckling deformation of a quarter of the perfect cylinder for (a) 51×101 mesh size and (b) 51×401 mesh size.

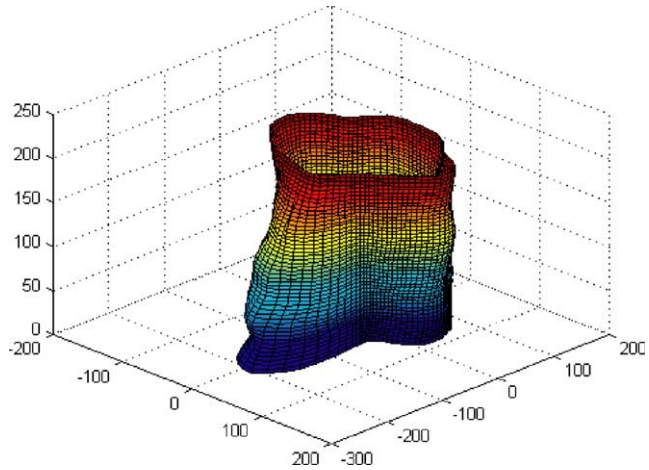

Fig. 20. Sample realization of non-homogeneous geometric imperfections using evolutionary power spectra and mesh 51×101.

stochastic field. Therefore, the mesh of 51×101 is considered adequate for providing sufficiently accurate predictions of the buckling load levels suitable for the comparative studies with respect to the buckling behaviour of the imperfect cylinder in the presence of additional sources of imperfections. For this example, the sample size used for the Monte Carlo simulation is taken $N_{\text{samp}} = 200$ which is considered sufficient for an accurate estimation of the mean value and standard deviation of the buckling loads.

6.2.1. Initial geometric imperfections

Fig. 21(a) presents the histogram of the buckling loads for the stochastic initial geometric imperfections generated using Eq. (14). For reasons of comparison, the loads are normalized by the predicted buckling load of the perfect cylinder using the mesh of 51×101, which is found to be $P_{\text{u}}^{(\text{perfect})} = 5650\,\text{N}$. The mean value and the coefficient of variation of the predicted buckling loads are found to be $\overline{P_{\text{u}}} = 4800\,\text{N}$ and 0.07548, respectively. This histogram is almost identical in shape with the results reported in [3]. However, a difference of about 15% in the calculated mean value is observed, which is roughly the same with the discretization error introduced by the the coarser mesh. This is a strong indication that the introduced error in the prediction of the buckling loads is a systematic discretization error, and the comparative studies using a coarser mesh, are reliable for this particular example. However, the validity of this assumption needs to be verified with a more systematic approach and will be the subject of a future research.

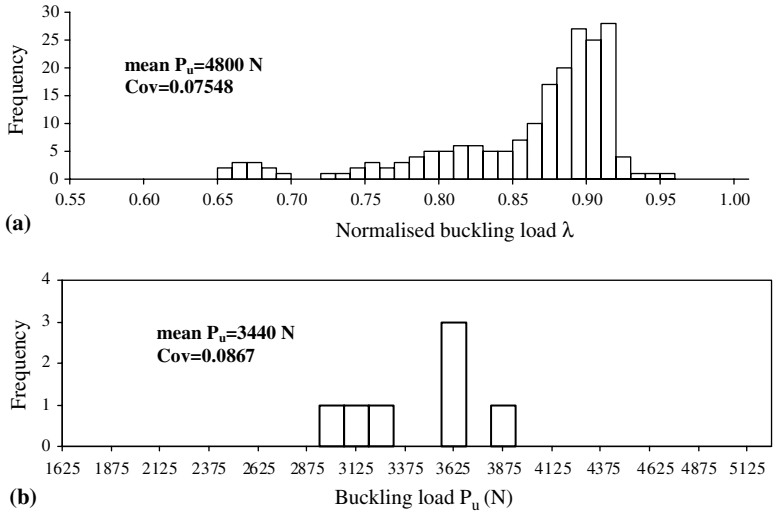

Fig. 21. Histograms of critical load factors: (a) 2D stochastic geometric imperfections; (b) experimental results (7 specimens [16]).

Fig. 21(b) presents the experimental results reported in [11]. The mean value of the measured experimental buckling loads is $\overline{P_u} = 3440\,\mathrm{N}$ and the coefficient of variation is 0.0867. From the comparison of Fig. 17(a) and (b) it can be observed that the shape of the predicted scatter of the buckling loads resembles the unimodal shape of the experimental results. In addition the predicted coefficient of variation is almost equal to the measured one. However, a difference is observed in the mean value of the predicted buckling loads, which is significantly larger than the measured one. This difference can be explained partially by the use of the coarser mesh, which systematically predicts higher levels of buckling loads and partially by the existence of other sources of imperfections such as material and thickness imperfections as well as uncertain boundary conditions and misalignment of vertical loads.

6.2.2. *Material and thickness imperfections*

In order to investigate the influence of material and thickness spatial variability on the buckling behaviour of the axially compressed cylinder, a preliminary parametric study of the buckling behaviour of the perfect cylinder is performed with respect to the correlation length parameters of the stochastic fields that describe the material and thickness variability, since no experimental data is available for the variability of these additional imperfection parameters. For this parametric study, the standard deviation is assumed to

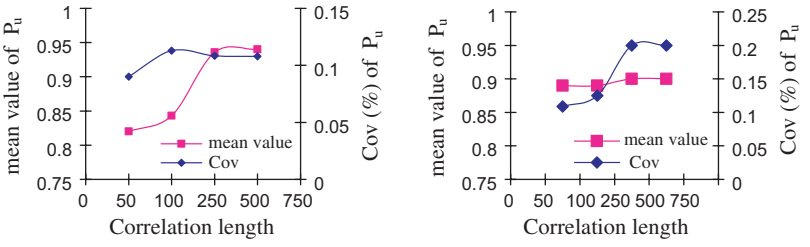

Fig. 22. Mean value and coefficient of variation (Cov) of the ultimate load P_u of the imperfect cylinder as a function of the correlation length parameters $b_1 = b_2$, for (a) 2D variation of the modulus of elasticity and (b) 2D variation of the thickness ($\sigma_f = 10\%$).

be 10% for both stochastic fields of modulus of elasticity and thickness, while it is assumed that the correlation length parameters are equal in both directions.

Fig. 22(a) and (b) presents the mean value and coefficient of variation of the ultimate load P_u of the perfect cylinder as a function of the correlation length parameters $b_1 = b_2$ of the modulus of elasticity and the thickness, respectively. From this figure it can be observed that the mean value of the predicted buckling loads remains constant and equal to $\overline{P_u} = 5085\,\mathrm{N}$, while the coefficient of variation reaches the values of 10% and 20% for a 2D variation of modulus of elasticity and thickness, respectively and for correlation lengths $b_1 = b_2 = 500\,\mathrm{mm}$. From this figure it can be seen that these additional sources of imperfections play an important role on the buckling behaviour of the cylinder even if they are considered as stand alone cases.

6.2.3. Combined geometric, material and thickness imperfections

Material and thickness imperfections are now combined and introduced simultaneously to the model of the imperfect cylinder. The standard deviation of the modulus of elasticity and the thickness are assumed to be 10% and 1%, respectively. These values for the standard deviation are in accordance with the corresponding measured values presented in Table 1. Fig. 23(a) and (b) present the histograms of the buckling loads of the cylinder for correlation lengths of modulus of elasticity and thickness $b_1 = b_2 = 50\,\mathrm{mm}$ and $b_1 = b_2 = 500\,\mathrm{mm}$, respectively. These correlation lengths were selected because, as shown in Fig. 22, they are responsible for the minimum and the maximum variance of the buckling loads of the perfect cylinder when material and thickness imperfections are considered as stand alone cases. The mean value of the predicted buckling loads is found to be $\overline{P_u} = 4250$ and $4550\,\mathrm{N}$, while the coefficient of variation is found to be 0.0945 and 0.1267 for $b_1 = b_2 = 50\,\mathrm{mm}$ and $b_1 = b_2 = 500\,\mathrm{mm}$, respectively. From this figure it can be seen that the basic unimodal shape of the predicted buckling loads observed in the stand alone case of initial geometric imperfections is preserved in the case of combined imperfections, while in the case of combined imperfections the prediction of the mean value is closer to the experimental results compared to the same prediction when only geometric imperfections are considered. In addition, larger correlation lengths of the material and thickness imperfections result in larger scatters of the predicted buckling loads.

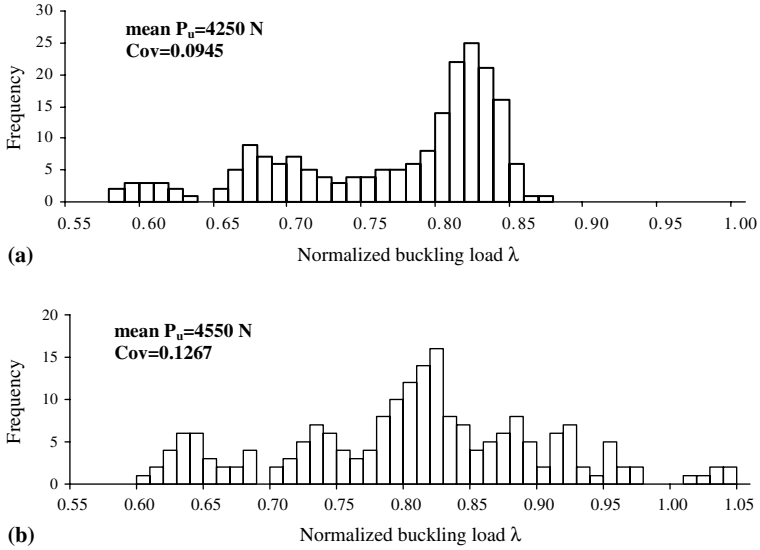

Fig. 23. Histograms of critical load factors for 2D combined imperfections: (a) correlation length of additional imperfections $b_1 = b_2 = 50\,\mathrm{mm}$ (b) correlation length of additional imperfections $b_1 = b_2 = 500\,\mathrm{mm}$.

7. Conclusions

In the present paper the effect of material and thickness imperfections on the buckling load of isotropic shells is investigated. For this purpose, the concept of an initial 'imperfect' structure is introduced involving not only geometric deviations of the shell structure from its perfect geometry but also a spatial variability of the modulus of elasticity as well as the thickness of the shell. These combined 'imperfections' are incorporated in an efficient and cost effective non-linear stochastic finite element formulation of the TRIC shell element using the local average method for the derivation of the stochastic stiffness matrix, while the variability of the limit loads is obtained by means of Monte Carlo Simulation procedure (MCS).

Using the proposed approach, the buckling behaviour of a cylindrical panel is investigated and compared to the results of a previous work by Papadopoulos and Papadrakakis [17] in which only geometric non-linearities were considered. The incorporation of the physical non-linearities to the non-linear analysis of this type of structures revealed the dominant role of the elastoplastic behaviour on the buckling analysis of imperfect cylindrical panels. A reduction of about 50% of the mean value of the buckling loads is computed in the elastoplastic panel with respect to the elastic one for the combined imperfections case, while the coefficient of variation remains almost the same. The introduction of 2D combined imperfections to the elastoplastic model increases four times the coefficient of variation of the buckling loads with respect to the stand-alone case. In this respect, the advantage of the decrease of the sensitivity of the elastoplastic panel to initial imperfections, which was exhibited in the stand-alone case (initial geometric imperfections only) as well as in the case of 1D combined imperfections, vanishes in the case of the most realistic 2D combined stochastic initial imperfections.

Furthermore, the investigation of the buckling behaviour of the axially compressed cylinder showed that the incorporation of material and thickness imperfections to the model of the non-homogeneous initial geometric imperfections resulted in close predictions of the distribution of the buckling loads of the cylinder with respect to the experimental results. More specifically, it is found that the basic unimodal shape of the predicted buckling loads observed in the stand alone case of initial geometric imperfections is preserved in the case of combined imperfections, while in the case of combined imperfections the prediction of the mean value is closer to the experimental results compared to the same prediction when only geometric imperfections are considered. In addition, larger correlation lengths of the material and thickness imperfections result in larger scatters of the predicted buckling loads. A further improvement of the prediction of the distribution of the buckling loads with respect to the shape of the scatter as well as to the mean value of the predicted buckling loads requires the incorporation of additional uncertain parameters such as boundary conditions and misalignment of the loading to the model of the initial 'imperfect' structure. The importance of these parameters should be the subject of a further study.

Acknowledgement

The authors would like to thank George Deodatis for his assistance in the implementation of the auto-regressive model with evolutionary power spectra.

References

[1] M. Deml, Wunderlich, Direct evaluation of the 'worst' imperfection shape in shell buckling, Comput. Methods Appl. Mech. Engrg. 149 (1997) 201–222.

[2] U. Albertin, W. Wunderlich, Buckling design of imperfect spherical shells, in: M. papadrakakis, A. Samartin, E. Onate (Eds.), Proc. of Fourth International Colloquium on Computation of Shell and Spatial Structures, in: IASS-IACM 2000, Chania—Crete, Greece.

[3] C.A. Schenk, G.I. Schueller, Buckling analysis of cylindrical shells with random geometric imperfections, Int. J. Non-Linear Mech. 38 (2003) 1119–1132.
[4] M.K. Chryssanthopoulos, C. Poggi, Probabilistic imperfection sensitivity analysis of axially compressed composite cylinders, Engng. Struct. 17 (6) (1995) 398–406.
[5] Y.W. Li, I. Elishakoff, J.H. Starnes Jr., D. Bushnell, Effect of the thickness variation and initial imperfection on buckling of composite shells: asymptotic analysis and numerical results by BOSOR4 and PANDA2, Int. J. Solids Struct. 34 (1997) 3755–3767.
[6] I. Elishakoff, Uncertain buckling: its past, present and future, Int. J. Solids Struct. 37 (2000) 6869–6889.
[7] G.V. Palassopoulos, Buckling analysis and design of imperfection sensitive structures, in: A. Haldar, A. Guran, B.M. Ayyub (Eds.), Uncertainty Modeling in Finite Element, Fatigue and Stability of Systems, Series on Stability, Vibration and Control of System Series B, vol. 9, World Scientific, Singapore, 1977, pp. 311–356.
[8] J.H. Argyris, L. Tenek, L. Olofsson, TRIC, a simple but sophisticated 3node triangular element based on 6 rigid-body and 12 straining modes for fast computational simulations of arbitrary isotropic and laminated composite shells, Comput. Methods Appl. Mech. Engrg. 145 (1997) 11–85.
[9] J.H. Argyris, L. Tenek, M. Papadrakakis, C. Apostolopoulou, Postbuckling performance of the TRIC natural mode triangular element for isotropic and laminated composite shells, Comput. Methods Appl. Mech. Engrg. 166 (1998) 211–231.
[10] J.H. Argyris, M. Papadrakakis, L. Karapitta, Elastoplastic analysis of shells with the triangular element TRIC, Comput. Methods Appl. Mech. Engrg. 191 (33) (2002) 3613–3637.
[11] J. Arbocz, H. Abramovich, The initial imperfection data bank at the Delft University of Technology Part 1, Technical Report LR-290, Department of Aerospace Engineering, Delft University of Technology, 1979.
[12] M. Shinozuka, Y. Sato, Simulation of nonstationary random processes, J. Engrg. Mech., ASCE EM1 (1967) 11–40.
[13] G. Deodatis, M. Shinozuka, Auto-regressive model for nonstationary stochastic processes, J. Engrg. Mech., ASCE 114 (11) (1988) 1995–2012.
[14] J. Lin, Y. Zhao, Y. Zhang, Accurate and highly efficient algorithms for structural stationary/non-stationary random responses, Comput. Methods Appl. Mech. Engrg. 191 (1–2) (2001) 103–111.
[15] J.H. Argyris, M. Papadrakakis, G. Stefanou, Stochastic finite element analysis of shells, Comput. Methods Appl. Mech. Engrg. 191 (41–42) (2002) 4781–4804.
[16] M. Shinozuka, G. Deodatis, Simulation of multi-dimensional Gaussian stochastic fields by spectral representation, Appl. Mech. Rev., ASME 49 (1996) 29–53.
[17] V. Papadopoulos, M. Papadrakakis, Finite element analysis of cylindrical panels with random initial imperfections, J. Engrg. Mech., ASCE 130 (8) (2004) 867–876.
[18] C.-C. Li, A. Der Kiureghian, An optimal discretization of random fields, Technical Report UCB/SEMM-92/04, Department of Civil Engineering, University of Berkeley, CA, USA, 1992.
[19] S. Lopez, Post-critical analysis of structures with a nonlinear pre-buckling state in the presence of imperfections, Comput. Methods Appl. Mech. Engrg. 191 (39–40) (2002) 4421–4440.